Simulation of Micromechanics of a Unidirectional Laminated Composite

Johnson Ezenwankwo[1,a], Yordan Kyosev[2,b], Iva Petríková[1,c] and Josef Žák[1,d]

[1]*Technical University of Liberec, 46117, Czech Republic;*
[2]*The Leibnitz Institute of Polymer Research, TU-Dresden, Dresden, Germany;*

[a]*johnson.ezenwankwo@tul.cz,* [b]*yordan.kyosev@tu-dresden.de,* [c]*iva.petrikova@tul.cz,*
[d]*josef.zak@tul.cz*

Abstract: Composite materials are among the most sought-after materials in major aerospace, automotive, naval applications of the 21st century. It is therefore paramount to conduct detailed materials analysis to obtain the elastic properties of attendant materials with respect to their dynamics in operation. This is technically cost-effective in eliminating repeated laboratory testing for very minute changes in input parameters. The model is a square-type unidirectional (UD) representative volume element (RVE) modelled in Abaqus CAE 6.14. An infinitesimal remote strain induced by means of a small displacement (15 - 20% of the boundary box length) from a reference/remote point tied kinematically and periodically to the face in question. The mesh sensitivity study was carried out in Ansys R22 because of its practical parametric sweep function, although mesh size was limited to 3 μm below which the number of nodes is not acceptable for the sake of license. The respective plots and attendant discussions are presented in the result section.

Keywords: Function; Unidirectional; Composites

1 Introduction

Composite materials have found widening applications in science and engineering. They present such technically desirable properties as good strength, low weight, high machinability, paths for innovative design changes, and corrosion resistance. They are not entirely devoid of challenges; their hydrophilic nature, high production cost and disposal problems are some areas that have bedevilled their usage [1]. Composites and their reinforcement textiles have vast application and scope; for example the weaving structure of warp knotted fabrics was extensively described by Kyosev Y. [2,3]. Reuss and Voigt proposed one of the earliest means of finding the mechanical properties of a composite in the rule of mixtures (ROM) [4,5]. In micromechanical analysis, homogenization is used to determine the engineering constants of a representative volume element (RVE). This is a fundamental step towards the practical design of composite structures and laminates [6]. The modified ROM was also developed to address the disagreement with experimental results. Other models for estimating the homogenized mechanical properties of an RVE exist. For the Young's modulus, shear modulus and Poisson's ratio, the homogenized orthotropic material properties are taken from literature [7]. The homogenized properties of an RVE are evaluated. To simplify the solutions, only the square-type model will be used; it is one of the simplest types of RVE when compared to randomly-distributed short fibres, particle fibres, hexagonal and diamond type. A mesh sensitivity study will be done using Ansys 2022 R2. This offers relative ease of manipulating the parametric sweep function of generating data of independent variables. Further future work will be on using the result obtained to perform a macromechanical analysis of a composite laminate plate of n-plies using safety factor (SF) and failure index (FI) as key performance indices for composite integrity. Input parameters are created as a text file and imported into the FEM platform at each required step. Several authors have expounded on laminated composites' micro and macromechnical analysis and

investigated their various failure models [8,9]. The very popular Chamis micromechanical model equations are widely employed to evaluate the RVE composite elastic properties. The idea being that both matrix and fibres are linear and elastic, and that the fibres are spacially distributed in a periodic fashion in either square or hexagonal type array [10,11]. In this study the Abaqus CAE tool is used to investigate the engineering constants of an RVE under the six standard load cases of tension in x, y and y – pure shear in xy, xz, xw. The Dirichlet boundary condition is imposed as against the periodic and Neumann boundary condition. The results obtained showed good agreement with the verified results from Python script developed by similar model [12].

2 FEM setup

2.1 Micromechanical analysis

The micromechanical analysis is performed using Abaqus CAE and the classic method of manually imposing periodic boundary condition (PBC) on a square type RVE in Abaqus and using a pre-existing plug-in [12] to compare the results obtained. Two models of same geometrics are generated using TexGen standalone open software and CMAS plug-in with Ansys r22. The latter showed better compatibility with other FEM tools, both for manually induced PBC and automatically-implemented ones through other plug-ins. The geometric properties are given in Table 1 below:

Table 1. RVE geometric properties.

	Domain		Fibre		$V_f \approx 0.448$
	(μm)				
	start	*end*	*start*	*end*	
X	0.0	100	0.0	100	D_f (μm) ≈ 75.7
Y	-50	50	0.0	0.0	
Z	-50	50	0.0	0.0	

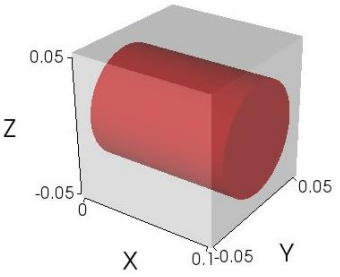

Fig. 1 Square-type RVE model (mm).

For all cases, the model is imported while retaining internal boundaries so that fibre and matrix can be assigned different material properties and selected as separate entities during the mesh creation process. The model from TexGen and Ansys r22 CMAS plug-in are exported as faceted models, as against smooth, since this improves the possibility of convergence during the solution. The following section will describe the implementation of periodic boundary condition (PBC) and sweep meshing sequences to ensure a conformal mesh on opposing sides of the model [13].

2.2 Periodic boundary condition and meshing

In mechanics of solids, the rule of thumb holds that the displacement vector component orthogonal to the plane of reference is zero. The rotational vector components parallel to the plane are also zero. But in solid models, rotational vector is not active; only the translational vector is considered. Periodic boundary condition (PBC) can be stated mathematically as follows:

$$r_i^a - r_i^b = 0, u_i^a = u_i^b + \bar{\varepsilon}_{ij}(x_j^a - x_j^b), \tag{1}$$

where *a* and *b* represent the corresponding surface pairs that describe the RVE, x_j is the distance between the opposite sides, u_i represents the displacement, and ε is the strain homogenous strain across the surface of the RVE. A critical part of the boundary condition is that the nodes along the symmetry plane for each case remained along the symmetry plane both before and after loading. For each simulation case, a total node-node constraint is applied to the symmetry plane, so there is no displacement in the direction perpendicular to the symmetry plane. An arbitrary plane is chosen as the symmetry plane and is retained for all conditions. In applying PBC, it is ensured that there exists equality in values of parameters on opposing edges that are *kinematically* linked to conform to the canonical equation in (1). This is typified by the idea that the meshing on each side of the geometry should be identical and conformal [14].

2.3 Material properties

The material properties of the matrix (modelled as Epoxy) and fibre (E-Glass) are given in the table below obtained from [8]. In a further work, the material property of the interface region will be modelled as data points of stress and their corresponding strain.

Table 2. Material properties.

	Matrix (Epoxy Resin)	**Fibre (E-Glass)**
Young's Modulus	3790 MPa	73000 MPa
Poisson's Ratio	0.35	0.22
Shear Modulus	4200 MPa	4345 MPa
Yield Strength	54.6 MPa	

3 Model setup

3.1 Using Abaqus CAE

In this method, the edges are tied all round with a representative loading condition whilst systematically excluding the three faces, XF, YT and ZF. Six sets capturing the faces of the RVE are creating at each loading front: X_{Front} (XF), X_{Back} (XB), Y_{Top} (YT), Y_{Base} (YB), Z_{Front} (ZF) and Z_{Back} (ZB).

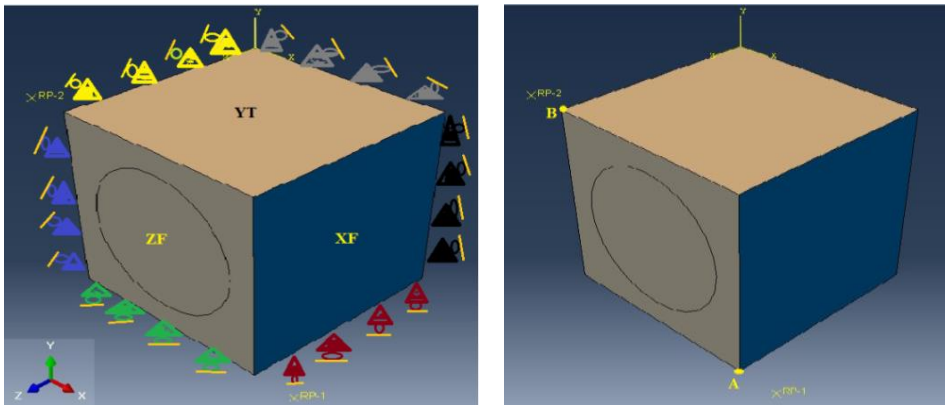

(a) (b)

Fig. 2 (a) Schematic of representative loading condition, (b) reference points (RF) A and B.

3.2 Meshing the part

Abaqus is equipped with one of the most efficient and accurate inbuilt meshing functions. Then a suitable element type is chosen. The number of divisions on each side of the cube representing the matrix can be seeded by parts or by edge length. If there is a remarkable size difference between constituent parts or deep contours which can present messing problems in some areas, the seeding could be done separately in parts, and *by parts* or by *edge length*. The mesh control option is used to determine the *element shape* and the *meshing technique* employed. The sweep technique is particular important for the periodic boundary condition so that there are identical meshing sequence on opposite face. The basic meshing metrics are shown below. Fig. 3 shows the periodic mesh of equal number of nodes on each pair opposite side.

Table 3. Meshing details.

Technique	Element Shape	Edge Length Division (mm)	Number of Divisions on Edge	Total Number of Elements:Nodes
Sweep	Hex/Hex dominated	0.005	= 0.1/0.005 = **20**	9560:10899

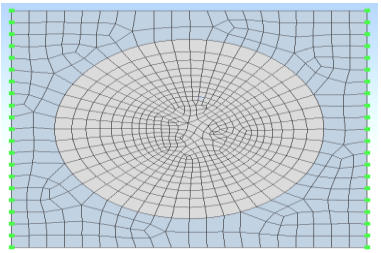

Fig. 3 Conformal periodic sweep mesh.

3.3 Reference loading

The reference points $X^{RP\text{-}1}$ and $X^{RP\text{-}2}$ are positioned at an arbitrarily small distance away (in this case 20 µm = 0.02 mm) from two chosen vertices whose coordinates are given in the *Table 2* below.

Table 4. Reference load points of Fig. 2b.

Vertex ID	Coordinates					
	x		y		z	
	Node	Load Point	Node	Load Point	Node	Load Point
A	0.1	0.12	-0.1	-0.1	0.1	0.1
B	0	-0.02	0	0	0.1	0.1
	Load Size					
Direction	(δ_x)	15 µm	(δ_y)	15 µm	(δ_y)	20 µm

Transverse Loading in x-direction

An infinitesimal displacement load of 12 µm is applied on the $X^{RP\text{-}1}$ (node A, Fig. 2b) while maintaining a linear constraint equation linking $X^{RP\text{-}1}$ with X_{Front} so that,

$$U(X)^{X_{Front}} = U(X)^{\text{XRP-1}} \tag{2}$$

The same is applied at X^{RP-2} and a third one at X^{RP-1} again for ZF at magnitudes of 15 μm and 20 μm respectively.

Transverse Loading in y-direction

Similarly, a reference point 2 (X^{RP-2}) is used to create a load location for the Y_{Top}. So that what is taking place at X^{RP-2} is transferred to the the Y_{Top} in that same direction.

$$U(Y)^{Y_{Top}} = U(Y)^{\text{XRP-2}} \tag{3}$$

Longitudinal Loading in z-direction

As in the cases of the X and Y fronts, a load which is tied to point 1(X^{RP-1}) is specifically oriented kinemtically so that its attributes are presented as loading in the z-direction as below. The load is upped by about 33%

$$U(Z)^{Z_{Front}} = U(Z)^{\text{XRP-1}} \tag{4}$$

4 Boundary condition

Restriction is needed to so that during loading only the side in question engages in displacement. Using the initial boundary condition for the uniaxial case, we fix XB in the x-direction, YB in the y-direction and ZB in the z-direction –all using roller boundary condition.

4.1 Constraint equations

The constraint equations are in agreement with those used to develop the Abaqus plug-in for RVE homogenization developed by Omairey S. And the periodicity condition in Digimat [12,15,16]. The constraint equations will involve actually implementing the relationships described in (1) – (4). A set of constraints is culled up using *equation* function in Abaqus. The first is to constrain the behaviour of XF WITH X^{RP-1}.

Table 5. Tensile load constrain equation variables on load points.

	x	**y**	**z**
Coefficient	1	1	1
	-1	-1	-1
Set Name	XF	YT	ZF
	X^{RP-1}	X^{RP-2}	X^{RP-1}
DOF	1	2	3
	1	2	3

Table 5 above captures the constraint equation variables for the infinitesimal representative loading in the x, y and z directions of the RVE. The negatives in the second terms of the coefficients come from moving the non-zero parameters to the left-hand side of the kinematic equation. The loading schematics and the boundary conditions are shown below in Fig. 4 where the reference points 1 and 2 are used to apply loading in the *x* and *z*, and then *y* directions, respectively.

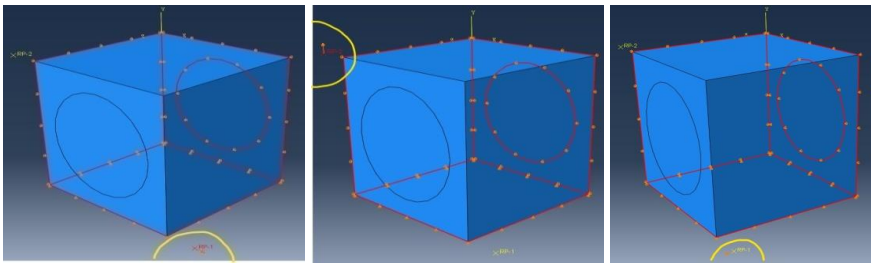

Fig. 4 Boundary condition and x, y and z loading.

4.2 Pure shear loading

Before discussing the result from the tension loading, it's worthy to expound on the concept of adding pure shear load to the RVE. For this, loads are simultaneously applied to the YZ-plane and XY-plane with respect to the X^{RP-1} and X^{RP-2} respectively. It is also pertinent to observe the care in positioning and directing the constituent loads that make up the shear components to accommodate for the y-bound force in the positive y direction and the x-bound force.

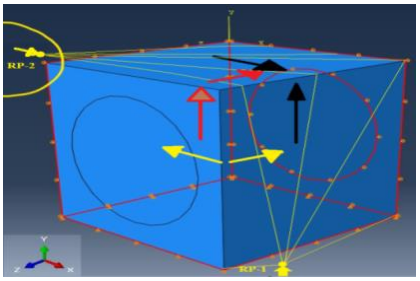

Fig. 5 Pure shear: τ_{xy}, τ_{xz} and τ_{yz} planes

The boundary condition involves imposing fixed constraints according to Table 6 below and then running separate simulations to obtain results for each case.

Table 6. Tensile load **c**onstrain equation variables on load points.

Pure Shear Direction	τ_{xy}		τ_{xz}		τ_{yz}	
Reference Side	YB	XB	*ZB*	*XB*	YB	ZB
Constrained Axis	*x, z*	*y, z*	*x, y*	*y, z*	*x, z*	*x, y*

As before, creating the correct boundary conditions plays a key role in ensuring accurate representation of a realistic model behaviour on which the results are hinged. For the first shear case (*XY* and *YX shear*), the boundary condition on the Y_{Base} and X_{Back} are that there are fixed constraints in the *x* and *z* directions, and then the y and z directions respectively. For the second shear case (*XZ* and *ZX shear*), the Z_{Back} and X_{Back} are fixed in the *x* and *z* directions, and then the y and z directions respectively, and finally, for the third case (*YZ* and *ZY shear*), the Y_{Base} and Z_{Back} are fixed in the *x* and *z* directions, and then the x and y directions respectively. All other variables not mentioned are not needed, and thus, are suppressed for the specific case. Tables 7 and 8 below show the shear load constrain dynamics and the load application schedule.

Table 7. Shear load constrain equation variables on load points.

Shear Equation Axes	XY	YX	XZ	ZX	YZ	ZY
Coefficient	1	1	1	1	1	1
	-1	-1	-1	-1	-1	-1
Set Name	X_{Front}	Y_{Top}	X_{Front}	Z_{Front}	Y_{Top}	Z_{Front}
	X^{RP-1}	X^{RP-2}	X^{RP-1}	X^{RP-2}	X^{RP-1}	X^{RP-2}
DOF	2	1	3	1	3	2
	2	1	3	1	3	2

Table 8. Reference shear load information.

Shear Load ID	XY	YX	XZ	ZX	YZ	ZY
Reference Point	X^{RP-1}	X^{RP-2}	X^{RP-1}	X^{RP-2}	X^{RP-1}	X^{RP-2}
Axis	+y	+x	+z	+x	+z	+y
Load Size	15 µm	15 µm	20 µm	15 µm	20 µm	15 µm

4.3 Mesh sensitivity study

Meshing a part is a vital part of FEM since it stems from the discretization of the geometry into smaller parts (elements) which are solved and generalized to give the result of the whole system. For this section, the Material Modeller built into newer versions Ansys is used. This is chosen because it offers great convenience in performing the needed parametric sweep of independent variables. Originally the model was meshed with a maximum mesh size of 5 µm. The sensitivity involved performing a sweep of parameters from 3 to 10 µm. The values remained remain tightly close with very infinitesimal margins.

Name	Values[0]	Values[1]	Values[2]	Values[3]	Values[4]	Values[5]	Values[6]	Values[7]	Values[8]	Values[9]	Unit
Image											
Parameters											
Fiber Volume Fraction	0.1	0.17222	0.24444	0.31667	0.38889	0.46111	0.53333	0.60556	0.67778	0.75	
Engineering Constants											
E1	10719	15722	20724	25725	30725	35725	40724	45724	50725	55730	MPa
E2	4796.7	5538.1	6440.2	7571.3	9009.1	10861	13294	16606	21424	29456	MPa
E3	4796.7	5538.1	6440.2	7571.3	9009.1	10861	13294	16606	21424	29456	MPa
G12	1684.9	1925.8	2208.2	2545	2956.3	3476	4164.6	5145.4	6725.9	10102	MPa
G23	1617.3	1780.1	1957.5	2159.1	2399.1	2700.1	3102.6	3690.4	4684.2	7070.1	MPa
G31	1684.9	1925.8	2208.2	2545	2956.3	3476	4164.6	5145.4	6725.9	10102	MPa
nu12	0.33396	0.32288	0.3122	0.30187	0.29184	0.28203	0.27231	0.26242	0.25195	0.24016	
nu13	0.33396	0.32288	0.3122	0.30187	0.29184	0.28203	0.27231	0.26242	0.25195	0.24016	
nu23	0.44531	0.44739	0.43381	0.41061	0.38032	0.34468	0.30563	0.26624	0.23245	0.218	

Fig. 6 Parametric sweet of the 5 µm mesh size.

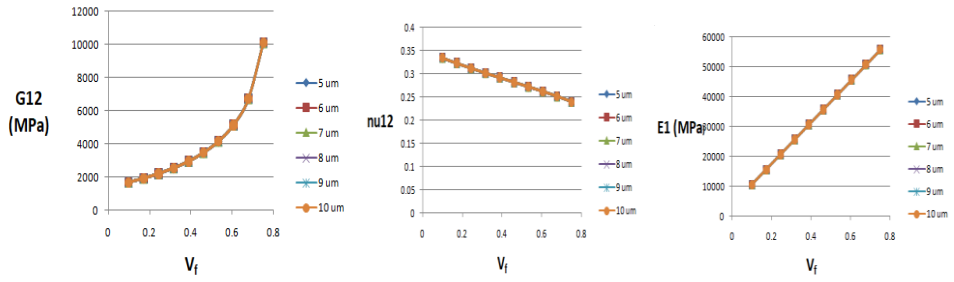

Fig. 7 Mesh sensitivity plot for G_{12}, nu_{12} and E_1.

5 Results and discussion

To present the results, the first idea is to plot the stress-strain curve for the three tensile load cases in X, Y and Z directions. Then a comparison is made of the plots of the shear cases considering the shear cases for each pair of planes (XY, YZ, and ZX planes). Stress-strain curve is obtained from the Abaqus post processor by invoking the excel plugin that exports the ramped-to-target-value data for the force and displacement. The stress and strain values are calculated from tables using the value of the measurement of the side of the bounding box (matrix) and consequently its cross-sectional area. The values of the Young's modulus are given in the table below and compared with results from a python-based Abaqus Plugin developed by Sadiq O. et al [12].

Table 9. Young's Modulus.

E_1		E_2		E_3	
Abaqus Simulation	Plugin (Abaqus)	Abaqus Simulation	Plugin (Abaqus)	Abaqus Simulation	Plugin (Abaqus)
7.0372GPa	10.10GPa	7.0049GPa	10.12GPa	32.926 GPa	32.915 GPa

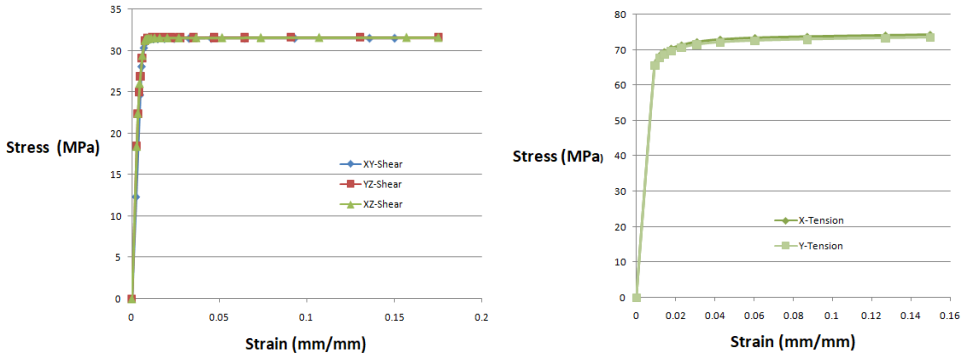

Fig. 8 Stress-strain result plots.

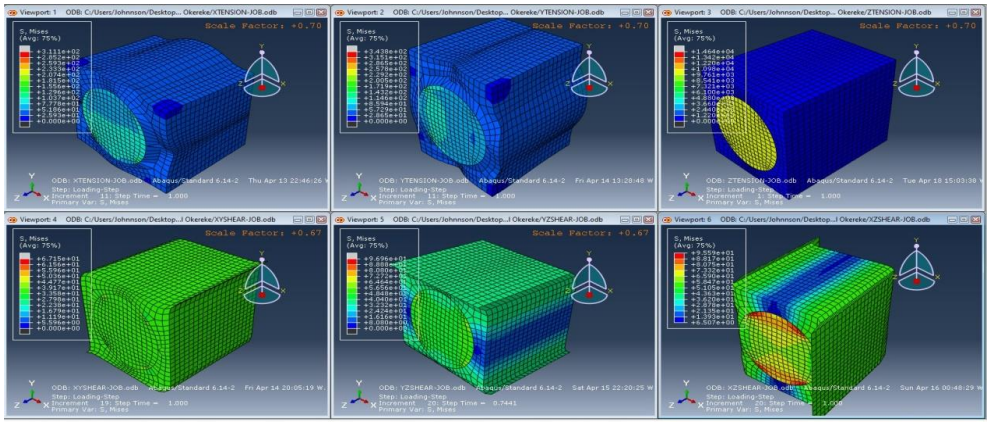

Fig. 9 Contour plots of the 6 load cases (*top row*: tension, *bottom row*: shear).

5.1 Stress and stain deliverables

Fig. 9 above shows the linked viewport of the 6 load cases. All components of stress *(s)*, strain *(E)*, reaction force *(RF)*, displacement *(u)* and plastic strain types *(PE, PEEQ and*

PEMAG) can be deduced from the virtualization tab. Loaded to the x-y plot function and exported as an excel file. The equivalent plastic strain is recorded as 1.5% while the von Mises stress is 311.1MPa for X-tension load case. The same is done for the remaining 5 load cases.

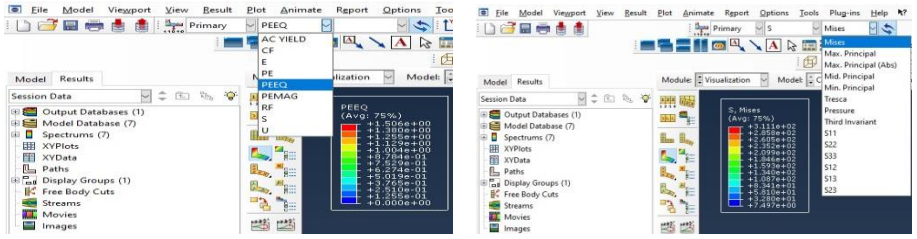

Fig. 10 Virtualization and exporting data points.

Conclusion

In general, Abaqus CAE among other tools has proven to be one of the best and user-friendly tools used by researchers and engineers alike in solving complex and delicate technical problems that require modelling and virtual solutions. Further work will involve incorporating the thermal aspect of response of UD RVE in Comsol Multiphysics and Digimat homogenization kit. As discussed earlier, modelling the interface and its plastic behaviours is one key aspect that further improves on the realistic approach of describing a UD-RVE.

Acknowledgement

This publication was written at the Technical University of Liberec as part of the project "Research of advanced materials, and application of machine learning in the area of control and modeling of mechanical systems" nr. SGS-2022-5072 with the support of the Specific University Research Grant, as provided by the Ministry of Education, Youth and Sports of the Czech Republic in the year 2022.

References

[1] Sathishkumar, T. P., Naveen, J. and Satheeskumar, S. “Hybrid fibre reinforced composites – a review,” *Journal of Reinforced Plastics and Composites*, **33**(5), pp. 454-471 (2014).

[2] Kyosev, K.K. *Warp Knitted Fabrics Construction*, (CRC Press, 1st Edition, 2019).

[3] Kyosev, K.K. “Process Based Method for Pattern Development of Narrow Woven Complex Profiles,” in *Advanced Weawing Technology*, Kyosev, K.K. and Bossou F. *eds.* (Springer Cham., Switzerland, 2022).

[4] Reuss, A. “Berechnung der Fließgrenze von Mischkristallen auf Grund der Plastizitätsbedingung für Einkristalle,” *Z angew Math Mech*, **9**(1), pp. 49-58 (1929). ISSN 1521-4001.

[5] Voigt, W. “Ueber die Beziehung zwischen den beiden Elasticitätsconstantenisotroper Körper,” *Annalen der physik*, **274**(12), pp. 573-587 (1889). ISSN 0003-4916.

[6] Yan C. “On the homogenization and de-homogenization of composite materials,” PhD Thesis, Drexel University, PA, USA, 2019.

[7] Tsai, S.W. and Hahn, H.T. *Introduction to composite materials* (CRC Press, 2018).

[8] Kaw, A.K. *Mechanics of composite materials* (Taylor & Francis Group, LLC, 2006).

[9] Chamis, C.C. “Simplified Composite Micromechanics Equations for Hygral, Thermal and Mechanical Properties,” in *Proceedings of the Anonymous Annual Conference of the Society of the Plastics Industry (SPI)*, Houston, USA, 1983, pp. 1-10.

[10] Voyiadjis, G.Z. and Kattan, P.I. *Mechanics of Composite Materials with MATLAB* (Springer, Germany, 1st Edition, 2005).

[11] Gay, D. Composite Materials: Design and Application (CRC Press; 3rd Edition, 2014).

[12] Omairey, S.L., Dunning, P.D. and Sriramula, S. “Development of an ABAQUS plugin tool for periodic RVE homogenization,” *Eng Comput*, **35**, pp. 567-577 (2019).

[13] Michael, O.I. and Akoyomare, A.I. "Virtual Framework for Prediction of the Full-Field Elastic Response of Unidirectional Composites," *Comp Mater Sci*, **70**, pp. 82-99 (2013).

[14] Nguyen, V.D., Bechet, E., Geuzaine, C. and Noels, L. "Imposing Periodic Boundary Condition on Arbitrary Meshes by Polynomial Interpolation", *Comp Mater Sci*, **55**, pp. 390-406 (2012).

[15] e-Xstream Engineering - Digimat, The Material Modeling Tool, May, *Available from* *http://www.e-xstream.com*., *Assessed* 2018-05-02.

[16] Xia, Z, Zhang, Y and Ellyin, F. “A Unified Periodical Boundary Conditions for Representative Volume Elements of Composites and Applications,” *Int J Solids Struct*, **40**(8), pp. 1907-1921 (2003).